






## Article

# Synthesis, Crystal Structure Analyses, and Antibacterial Evaluation of the Cobalt(II) Complex with Sulfadiazine-Pyrazole Prodrug

Mezna Saleh Altowyan <sup>1</sup>, Matti Haukka <sup>2</sup>, Mohammed Salah Ayoup <sup>3</sup>, Magda M. F. Ismail <sup>4</sup>, Nagwan G. El Menofy <sup>5</sup>, Saied M. Soliman <sup>3,\*</sup>, Assem Barakat <sup>6</sup>, Mona M. Sharaf <sup>7</sup>, Morsy A. M. Abu-Youssef <sup>3,\*</sup> and Amal Yousri <sup>3,\*</sup>

<sup>1</sup> Department of Chemistry, College of Science, Princess Nourah bint Abdulrahman University, P.O. Box 84428, Riyadh 11671, Saudi Arabia; msaltowyan@pnu.edu.sa

<sup>2</sup> Department of Chemistry, University of Jyväskylä, P.O. Box 35, FI-40014 Jyväskylä, Finland; matti.o.haukka@jyu.fi

<sup>3</sup> Department of Chemistry, Faculty of Science, Alexandria University, Ibrahimia, P.O. Box 426, Alexandria 21321, Egypt; mohamed.salah@alexu.edu.eg

<sup>4</sup> Department of Pharmaceutical Medicinal Chemistry, Faculty of Pharmacy (Girls), Al-Azhar University, Cairo 11884, Egypt; magdaismail@azhar.edu.eg

<sup>5</sup> Department of Microbiology and Immunology, Faculty of Pharmacy (Girls), Al-Azhar University, Cairo 11884, Egypt; nagwan.elmenofy@azhar.edu.eg

<sup>6</sup> Department of Chemistry, College of Science, King Saud University, P.O. Box 2455, Riyadh 11451, Saudi Arabia; ambarakat@ksu.edu.sa

<sup>7</sup> Protein Research Department, Genetic Engineering and Biotechnology Research Institute, City of Scientific Research and Technological Applications, Alexandria P.O. Box 21933, Egypt; sharafmona4@gmail.com

\* Correspondence: saiedsoliman@yahoo.com (S.M.S.); morsy5@alexu.edu.eg (M.A.M.A.-Y.); amal.yousri@alexu.edu.eg (A.Y.)



**Citation:** Altowyan, M.S.; Haukka, M.; Ayoup, M.S.; Ismail, M.M.F.; El Menofy, N.G.; Soliman, S.M.; Barakat, A.; Sharaf, M.M.; Abu-Youssef, M.A.M.; Yousri, A. Synthesis, Crystal Structure Analyses, and Antibacterial Evaluation of the Cobalt(II) Complex with Sulfadiazine-Pyrazole Prodrug. *Inorganics* **2023**, *11*, 382. <https://doi.org/10.3390/inorganics11100382>

Academic Editor: Vladimir Arion

Received: 9 August 2023

Revised: 21 September 2023

Accepted: 22 September 2023

Published: 25 September 2023



**Copyright:** © 2023 by the authors. Licensee MDPI, Basel, Switzerland. This article is an open access article distributed under the terms and conditions of the Creative Commons Attribution (CC BY) license (<https://creativecommons.org/licenses/by/4.0/>).

**Abstract:** The complex  $[\text{Co}(\text{L})(\text{H}_2\text{O})_4](\text{NO}_3)_2$  of (*E*)-4-(2-(3-methyl-5-oxo-1-(pyridin-2-yl)-1*H*-pyrazol-4(5*H*)-ylidene)hydrazinyl)-*N*-(pyrimidin-2-yl)benzenesulfonamide (**L**) was synthesized via the self-assembly technique. Its molecular and supramolecular structures were analyzed using FTIR, elemental analyses, and single-crystal X-ray diffraction, as well as Hirshfeld calculations. This complex crystallized in the triclinic space group  $P\bar{1}$  with  $Z = 2$ . The crystallographic asymmetric unit comprised one complex cation and two nitrate counter anions. This complex had distorted octahedral geometry around the Co(II) ion. Numerous intermolecular interactions affecting the molecular packing of this complex were conformed using Hirshfeld investigations. The most significant contacts for the cationic inner sphere  $[\text{Co}(\text{L})(\text{H}_2\text{O})_4]^{2+}$  were  $\text{O}\cdots\text{H}$  (38.8%),  $\text{H}\cdots\text{H}$  (27.8%), and  $\text{N}\cdots\text{H}$  (9.9%). On the other hand, the main interactions for the counter  $\text{NO}_3^-$  ions were the  $\text{O}\cdots\text{H}$  (79.6 and 77.8%),  $\text{O}\cdots\text{N}$  (8.0%), and  $\text{O}\cdots\text{C}$  (9.1%). A high propensity for making interactions for each atom pair in the contacts  $\text{O}\cdots\text{H}$ ,  $\text{N}\cdots\text{C}$ ,  $\text{N}\cdots\text{H}$ , and  $\text{C}\cdots\text{C}$  was revealed by enrichment ratio values greater than 1. The antibacterial efficacy of the complex and the free ligand were assessed. The free ligand had higher antibacterial activity ( $\text{MIC} = 62.5\text{--}125\text{ }\mu\text{g/mL}$ ) than the  $[\text{Co}(\text{L})(\text{H}_2\text{O})_4](\text{NO}_3)_2$  complex ( $\text{MIC} \geq 250\text{ }\mu\text{g/mL}$ ) versus all the studied bacteria.

**Keywords:** Co(II) coordination complex; self-assembly; X-ray; Hirshfeld analysis; antibacterial evaluation; sulfadiazine

## 1. Introduction

The design of novel drugs is complicated and challenge due to bacterial antibiotic resistance mechanisms. A prodrug that relies on bacterial enzymes to release the active drug at the site of infection can be used as an antibacterial agent [1,2]. Prodrugs also have the potential to improve the pharmacological characteristics of the parent drug molecule. Sulfonamides (sulfanilamides) are among the most commonly used antibiotics in the

world, primarily due to their high efficiency against bacterial infections, low cost, and minimal toxicity [3,4]. A number of possible donor atoms, including  $N_{(\text{amino})}$ ,  $N_{(\text{pyrimido})}$ ,  $N_{(\text{sulfonamido})}$ , and  $O_{(\text{sulfonyl})}$  atoms, are present in sulfonamides, making them highly flexible chelating agents [5]. Sulfadiazine is a sulfanilamide which possesses several coordination modes and can act as a monodentate [6], bidentate [7], or bridging ligand via the *N*-atoms of the pyrimidine ring [8]. Sulfadiazine is used to treat several parasitic diseases, such as malaria and toxoplasmosis, in addition to urinary tract infections [9]. In addition, Sulfadiazine is broadly used as an efficient antibacterial agent for both Gram-positive and Gram-negative bacteria [10]. Interestingly, ligands rich with nitrogen as donor atoms (such as pyrazole and pyridine) are capable of coordinating with different metal ions to yield highly stable metal complexes. Pyrazole is one of the most flexible substances in inorganic chemistry due to its interesting coordination chemistry with different transition metals [11]. Furthermore, its high thermal stability is the most advantageous for its use in many synthetic methods [12]. Pyrazole derivatives are applied widely in many aspects, such as in catalysis and supramolecular chemistry [13]. Additionally, pyridine derivatives have been broadly applied in the field of medicinal drugs [14]. By adding a pyrazole moiety to the sulfadiazine, we designed, produced, and published a new prodrug [15].

Recently, the application of metal complexes in medicine, especially in cancer therapy [16–18], bacterial infection treatment [19,20], and as antifungal agents [21,22], has attracted widespread interest. In particular, metal complexes of sulfadiazine have drawn much attention by many researchers [23–26]. These complexes are broadly used as antimicrobial agents, such as silver, zinc, cerium, and cobalt sulfadiazine. Silver sulfadiazine is a good example of an antimicrobial agent for wound healing in the case of burns [27]. Silver sulfadiazine cream is the most widely used cream for treating burns, with sodium sulfadiazine and silver nitrate as its active substances [28]. Furthermore, burned animals are treated with zinc sulfadiazine to avoid infection caused by bacteria. Cobalt(II) sulfadiazine has proven to be as effective as Zn(II) and Ce(III) sulfadiazine at healing burns in rats [29]. Cobalt(II) sulfadiazine complexes have displayed different coordination geometries. Two cobalt(II) complexes of the antibiotic sulfadiazine were studied by Ajibade et al. [30], both of which were six-coordinate. The one that was crystallographically characterized revealed a centrosymmetric 3D structure with a bidentate coordination of the sulfadiazine ligand in the equatorial plane using sulfonamide and pyrimidine nitrogen donor atoms, while the axial position was occupied by a methanol oxygen donor atom; the donor atoms of each kind in the distorted octahedral geometry were related by a center of inversion. Another Co(II) sulfadiazine complex, in which the Co(II) ion was surrounded by a rectangular bipyramid environment, was presented by Gil and coworkers [31]. In addition, other cobalt(II) sulfadiazine complexes have been reported to exist as mononuclear [25,32], trinuclear [33], tetranuclear [8], and hexanuclear [33] complexes.

Thus, our research focused on the use of the sulfadiazine-pyrazole prodrug (*E*)-4-(2-(3-methyl-5-oxo-1-(pyridin-2-yl)-1*H*-pyrazol-4(5*H*)-ylidene)hydrazinyl)-*N*-(pyrimidin-2-yl)-benzenesulfonamide (**L**; Figure 1) [15] as a ligand (**L**) in combination with cobalt(II) nitrate hexahydrate for the synthesis of a new coordination complex via the self-assembly method. The newly synthesized complex was characterized using the FTIR spectroscopic technique and an elemental analysis. Moreover, the structure of this complex was determined definitively using single-crystal X-ray analyses; the intermolecular forces in the crystal lattice were investigated using Hirshfeld calculations. Additionally, an antibacterial evaluation was performed for the ligand and its new Co(II) complex.

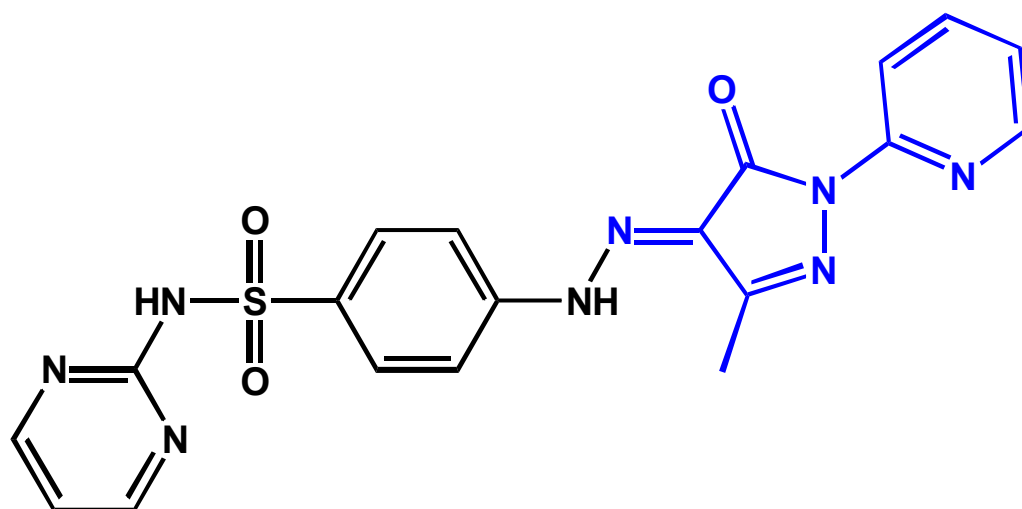


**Figure 1.** Structure of (*E*)-4-(2-(3-methyl-5-oxo-1-(pyridin-2-yl)-1*H*-pyrazol-4(5*H*)-ylidene)hydrazinyl)-*N*-(pyrimidin-2-yl)benzenesulfonamide (**L**).

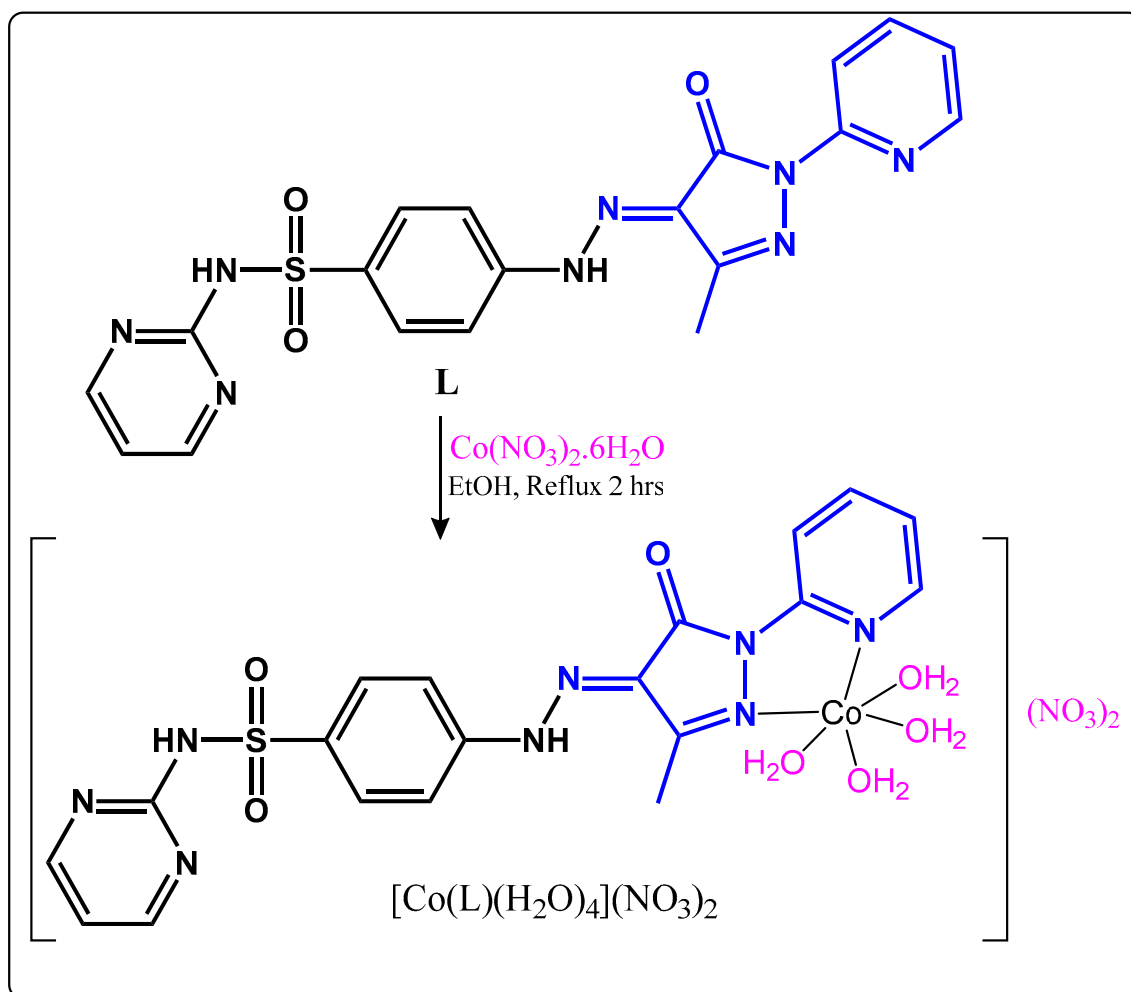
## 2. Results and Discussion

### 2.1. Synthesis and Characterization

The studied  $[\text{Co}(\text{L})(\text{H}_2\text{O})_4](\text{NO}_3)_2$  complex was synthesized using the self-assembly method. The ethanolic solutions of both  $\text{Co}(\text{NO}_3)_2 \cdot 6\text{H}_2\text{O}$  and the ligand were mixed and refluxed for 2 h (Scheme 1). The resulting clear, dark pink mixture was allowed to evaporate at room temperature. After four weeks, this complex was formed as dark pink crystals that could be used for the single-crystal X-ray diffraction analysis. FTIR spectra and elemental analyses were used to confirm the structure. There were some variations in the FTIR spectra of this complex compared to the FTIR spectra of the free ligand (Figure S1 in Supplementary Materials), confirming the coordination between the Co(II) ion and the free ligand. The broad absorption band at  $3391\text{ cm}^{-1}$  in the FTIR spectra of the Co(II) complex confirmed the existence of  $\text{H}_2\text{O}$  molecules. This vibrational band was not detected in the FTIR spectra of the free ligand. In the FTIR spectra of the free ligand, the band observed at  $3430\text{ cm}^{-1}$  was assigned to the N-H vibration, while the bands observed at  $3071$  and  $3021\text{ cm}^{-1}$  could be assigned to the aromatic C-H vibrational bands, and aliphatic C-H vibrational bands were observed at  $2927$  and  $2864\text{ cm}^{-1}$ . These aromatic and aliphatic C-H vibrational bands, as well as the N-H vibrational band, were masked by a broad O-H band in the FTIR spectra of the complex. In addition, the  $\nu(\text{C}=\text{O})$  was detected at  $1679$  and  $1675\text{ cm}^{-1}$  in the free ligand and its Co(II) complex, respectively. The coordination of the Co(II) ion via the  $\text{N}_{(\text{pyridine})}$  and the  $\text{N}_{(\text{pyrazole})}$  atoms was indicated by the shifts of the imine vibration, as well as the aromatic ring's carbon–carbon and carbon–nitrogen vibrations. The former was detected at  $1624\text{ cm}^{-1}$ , while the latter was detected in the region of  $1551$ – $1483\text{ cm}^{-1}$  in the Co(II) complex. The respective values for the free ligand were observed at  $1598$  and  $1551\text{ cm}^{-1}$ . Additionally, a sharp peak appeared at  $1383\text{ cm}^{-1}$ , representing the stretching modes of the  $\text{NO}_3^-$  vibrations in the Co(II) complex, but in the free ligand spectra, this peak was not observed. The  $[\text{Co}(\text{L})(\text{H}_2\text{O})_4](\text{NO}_3)_2$  complex was found to be soluble in ethanol, methanol, acetonitrile, DMSO, and DMF, but insoluble in water.

### 2.2. X-ray Structure Description

Single-crystal X-ray crystallography was used to conclusively determine the structure of  $[\text{Co}(\text{L})(\text{H}_2\text{O})_4](\text{NO}_3)_2$ . This complex crystallized in the low-symmetry triclinic crystal system and  $P\bar{1}$  space group. The unit cell parameters were  $a = 7.73330(10)\text{ \AA}$ ,  $b = 12.5152(2)\text{ \AA}$ ,  $c = 15.5216(2)\text{ \AA}$ ,  $\alpha = 76.2120(10)^\circ$ ,  $\beta = 77.9620(10)^\circ$ , and  $\gamma = 78.9690(10)^\circ$ . The volume of the unit cell was  $1410.92\text{ \AA}^3$  and  $Z = 2$ . Figure 2 displays the asymmetric unit of the studied complex, while the selected bond lengths and angles are presented in Table 1.



**Scheme 1.** Synthesis of  $[\text{Co}(\text{L})(\text{H}_2\text{O})_4](\text{NO}_3)_2$  complex.

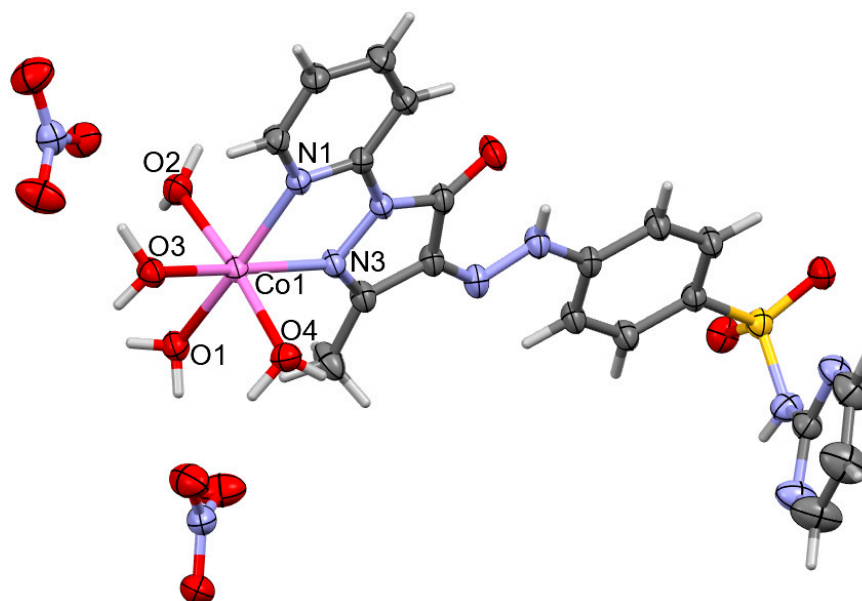


**Figure 2.** Structure of the asymmetric unit of  $[\text{Co}(\text{L})(\text{H}_2\text{O})_4](\text{NO}_3)_2$  with atom numbering. Thermal ellipsoids are at the 50% probability level. Atom color codes are: Co: purple; O: red; N: blue; C: dark grey; H: light grey; and S: yellow.

**Table 1.** Selected bond lengths (Å) and angles (°) for [Co(L)(H<sub>2</sub>O)<sub>4</sub>](NO<sub>3</sub>)<sub>2</sub> complex.

| Bond            | Distance   | Bond            | Distance   |
|-----------------|------------|-----------------|------------|
| Co(1)-O(2)      | 2.0635(11) | Co(1)-O(1)      | 2.1036(10) |
| Co(1)-O(4)      | 2.0909(11) | Co(1)-N(1)      | 2.1240(10) |
| Co(1)-O(3)      | 2.0986(10) | Co(1)-N(3)      | 2.1406(10) |
| Bonds           | Angle      | Bonds           | Angle      |
| O(2)-Co(1)-O(4) | 174.25(4)  | O(3)-Co(1)-N(1) | 96.86(4)   |
| O(2)-Co(1)-O(3) | 90.11(4)   | O(1)-Co(1)-N(1) | 170.36(4)  |
| O(4)-Co(1)-O(3) | 86.97(4)   | O(2)-Co(1)-N(3) | 94.99(4)   |
| O(2)-Co(1)-O(1) | 85.00(5)   | O(4)-Co(1)-N(3) | 88.51(4)   |
| O(4)-Co(1)-O(1) | 90.00(4)   | O(3)-Co(1)-N(3) | 171.61(4)  |
| O(3)-Co(1)-O(1) | 89.31(4)   | O(1)-Co(1)-N(3) | 97.76(4)   |
| O(2)-Co(1)-N(1) | 87.57(4)   | N(1)-Co(1)-N(3) | 76.74(4)   |
| O(4)-Co(1)-N(1) | 97.69(4)   |                 |            |

In the cationic inner sphere [Co(L)(H<sub>2</sub>O)<sub>4</sub>]<sup>2+</sup>, the Co(II) ion was hexa-coordinated with four O-atoms from four H<sub>2</sub>O molecules, where the Co-O distances were within the range of 2.0635(11)–2.1036(10) Å. In addition, the Co(II) was coordinated with one unit of the ligand via pyridine (N1) and pyrazole (N3) atoms. Hence, the ligand acted as a bidentate *NN*-chelate. The Co(1)-N(1) and Co(1)-N(3) bond distances were 2.1240(10) and 2.1406(10) Å, respectively, where the Co-N<sub>(pyrazole)</sub> bond distance was slightly larger than the Co-N<sub>(pyridine)</sub> one. The bite angle N(1)-Co(1)-N(3) of the ligand was 76.74(4)°. The angles of O(2)-Co(1)-O(4), O(1)-Co(1)-N(1), and O(3)-Co(1)-N(3) were found to be 174.25(4)°, 170.36(4)°, and 171.61(4)°, respectively, which were all deviated from the ideal value of 180°. As a result, a distorted octahedral coordination geometry for this complex was observed. The weak ligand-field strength resulting from the four aqua ligands and the pyridyl-pyrazole coordination moiety of the sulfadiazine indicated that the complex was in the high-spin state. In the high-spin complexes [Co(1-[3-(2-pyridyl)-pyrazol-1-ylmethyl]-naphthalene)<sub>3</sub>](ClO<sub>4</sub>) [34] and [Co(3-phenyl-5-(2-pyridyl)pyrazole)<sub>2</sub>Cl(H<sub>2</sub>O)]Cl·H<sub>2</sub>O [35], the Co-N distances were 2.122(4)–2.213(4) Å [35] and 2.1035(19)–2.1831(19) Å [34], respectively, while the Co-O distance was 2.0845(18) Å [35]. These values confirmed the high-spin state of the studied complex.

It is important to notice that the pyridine ring and adjacent pyrazole ring were slightly not co-planar to each other, with a twist angle of 1.68(3)°. In comparison to the free ligand, the twist angle between these two rings was 6.45° [15]. Hence, the coordination between Co(II) and the N-atoms of the pyridine and pyrazole rings increased the co-planarity of the two ring systems. The two nitrate ions represented the outer sphere of this complex, which participated significantly in the supramolecular structure of this complex. The molecular packing of this complex was controlled by significant O-H···O and N-H···O hydrogen bonding contacts, which are shown in Figure 3. Their corresponding geometric parameters are listed in Table 2.

**Table 2.** The geometric parameters of the O-H···O and N-H···O contacts in [Co(L)(H<sub>2</sub>O)<sub>4</sub>](NO<sub>3</sub>)<sub>2</sub> complex.

| D-H···A            | d(D-H)/Å | d(H···A)/Å | d(D···A)/Å | <(DHA)/° | Symm. Code      |
|--------------------|----------|------------|------------|----------|-----------------|
| O(1)-H(1B)···O(7)  | 0.80(3)  | 2.06(3)    | 2.8154(14) | 159(2)   | x − 1, y − 1, z |
| O(1)-H(1A)···O(11) | 0.84(2)  | 1.92(3)    | 2.7190(18) | 159(2)   |                 |
| O(2)-H(2B)···O(8)  | 0.81(3)  | 2.03(3)    | 2.8323(17) | 171(2)   | −x, −y, −z      |
| O(2)-H(2A)···O(10) | 0.84(2)  | 2.02(2)    | 2.8583(19) | 174(2)   | x + 1, y, z     |
| O(3)-H(3B)···O(8)  | 0.96(3)  | 1.78(3)    | 2.7352(16) | 170(2)   |                 |
| O(4)-H(4A)···O(12) | 0.92(3)  | 1.90(3)    | 2.8135(17) | 172(3)   |                 |
| O(4)-H(4B)···O(13) | 0.75(3)  | 2.05(3)    | 2.7922(18) | 168(3)   | −x, −y, −z + 1  |
| N(5)-H(5)···O(5)   | 0.77(2)  | 2.13(2)    | 2.7657(16) | 139(2)   |                 |

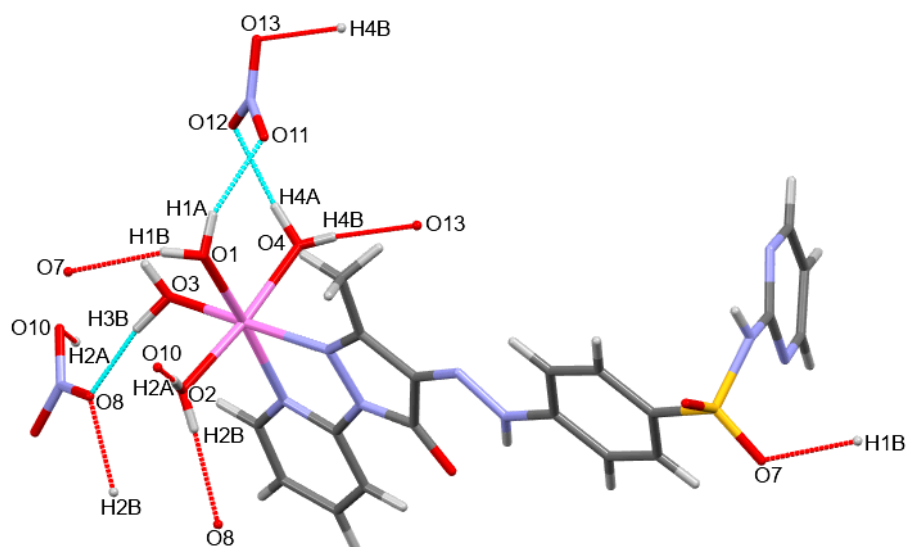


**Figure 3.** The important O-H $\cdots$ O and N-H $\cdots$ O contacts in the crystal structure of [Co(L)(H<sub>2</sub>O)<sub>4</sub>](NO<sub>3</sub>)<sub>2</sub> complex.

The supramolecular structure of this complex was stabilized by O(1)-H(1A) $\cdots$ O(11), O(3)-H(3B) $\cdots$ O(8), and O(4)-H(4A) $\cdots$ O(12) intramolecular hydrogen bonding contacts with donor to acceptor distances of 2.7190(18), 2.7352(16), and 2.8135(17) Å, respectively. Additionally, the molecular packing was controlled by the O(1)-H(1B) $\cdots$ O(7) intermolecular hydrogen bonding interactions, in which the donor O(1) to acceptor O(7) distance was 2.8154(14) Å, while the O(1)-H(1B) $\cdots$ O(7) angle was 159(2)°. The resulting packing scheme via these O-H $\cdots$ O and N-H $\cdots$ O contacts is shown in Figure 4A. Furthermore, the C(5) $\cdots$ C(15) interactions depicted in Figure 4B are an indication for the existence of aromatic  $\pi$ - $\pi$  stacking interactions between the monomeric complex units. The C(5) $\cdots$ C(15) interaction distance was 3.37(2) Å.

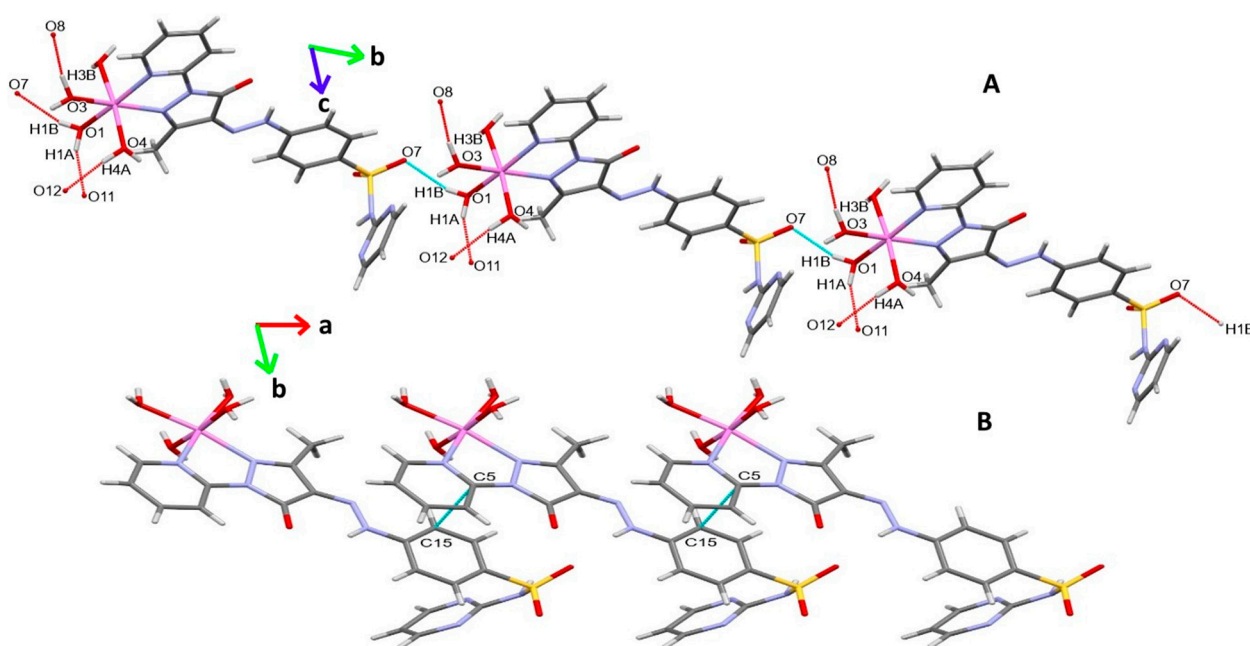


**Figure 4.** Packing scheme of the [Co(L)(H<sub>2</sub>O)<sub>4</sub>](NO<sub>3</sub>)<sub>2</sub> complex via O-H $\cdots$ O and N-H $\cdots$ O interactions along *bc* plane (A) and  $\pi$ - $\pi$  stacking interactions along *ab* plane (B) in this complex.



### 2.3. Molecular Packing Analysis

An easy and precise method for identifying the various interactions between the atoms in a crystal structure is a Hirshfeld topology analysis. It was used to decompose the intermolecular interactions occurring in the crystal structure of the  $[\text{Co}(\text{L})(\text{H}_2\text{O})_4](\text{NO}_3)_2$  complex. The cationic inner sphere  $[\text{Co}(\text{L})(\text{H}_2\text{O})_4]^{2+}$  was surrounded by two nitrate anions in the crystal structure of the  $[\text{Co}(\text{L})(\text{H}_2\text{O})_4](\text{NO}_3)_2$  complex. Therefore, the Hirshfeld surfaces of the cationic part (F1) and the two counter anions (F2 and F3) were analyzed independently. In Figure 5, the generated Hirshfeld maps are displayed.

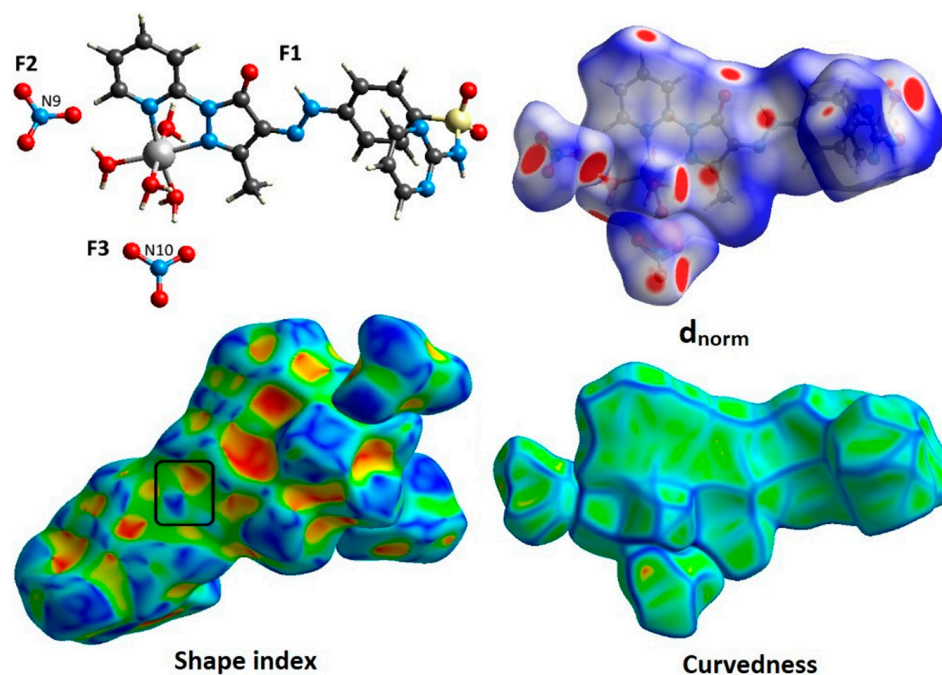


**Figure 5.** Hirshfeld surfaces mapped over  $d_{\text{norm}}$ , shape index, and curvedness for the studied three fragments (F1 to F3) of  $[\text{Co}(\text{L})(\text{H}_2\text{O})_4](\text{NO}_3)_2$  complex.

The percentage contributions of the different intermolecular contacts for the two fragments (F2 and F3), as well as the cationic part (F1), are presented in Table 3. Although the nitrate counter anions did not participate in the complex's coordination sphere, they contributed strongly to the intermolecular contacts, as shown in Table 3. According to the percentages obtained from fingerprint plots, the F2 and F3 fragments of the two nitrate anions shared slightly different intermolecular contacts.

**Table 3.** The percentages of all potential interactions in  $[\text{Co}(\text{L})(\text{H}_2\text{O})_4](\text{NO}_3)_2$  complex.

| Contact | %Contact  |                      |                      |
|---------|---|----------------------|----------------------|
|         | $[\text{Co}(\text{L})(\text{H}_2\text{O})_4]^{2+}$ (F1) | $\text{NO}_3^-$ (F2) | $\text{NO}_3^-$ (F3) |
| O...O   | 0.9   | 2.9                  | 1.8                  |
| O...N   | 2.1   | 8.0                  | 7.2                  |
| O...C   | 5.2   | 5.2                  | 9.1                  |
| O...H   | 38.8  | 79.6                 | 77.8                 |
| N...N   | 0.6   | 0                    | 1.3                  |
| N...C   | 2.3   | 0.5                  | 0.6                  |
| N...H   | 9.9   | 3.8                  | 2.2                  |
| C...C   | 2.4   | 0                    | 0                    |
| C...H   | 10  | 0                    | 0                    |
| H...H   | 27.8  | 0                    | 0                    |

Numerous short interactions, including O $\cdots$ H, H $\cdots$ H, and N $\cdots$ H interactions, were found to play major roles in controlling the packing of the cationic part of this complex. Their percentages were estimated to be 38.8, 27.8, and 9.9%, respectively. In addition, other short contacts (O $\cdots$ C, C $\cdots$ C, and O $\cdots$ N) participated in the packing of this complex, with smaller percentages of 5.2, 2.4, and 2.1%, respectively. On the other hand, the O $\cdots$ H (79.6%) and O $\cdots$ N (8.0%) contacts for fragment **F2** were the major interactions. For fragment **F3**, the significant contacts were O $\cdots$ H (77.8%) and O $\cdots$ C (9.1%). These interactions represent the short contacts, since they appeared as red areas in the  $d_{\text{norm}}$  map, as well as sharp spikes in the fingerprint plots, as shown in Figures 6 and 7, respectively. All the other interactions were of less importance and were often weak, as they appeared as white and blue areas in the  $d_{\text{norm}}$  map. In the shape index map, red and blue triangles are observed, indicating aromatic  $\pi$ - $\pi$  stacking interactions. The flat green areas in the curvedness map additionally supported the presence of  $\pi$ - $\pi$  stacking interactions. The percentage of C $\cdots$ C interactions was 2.4%.

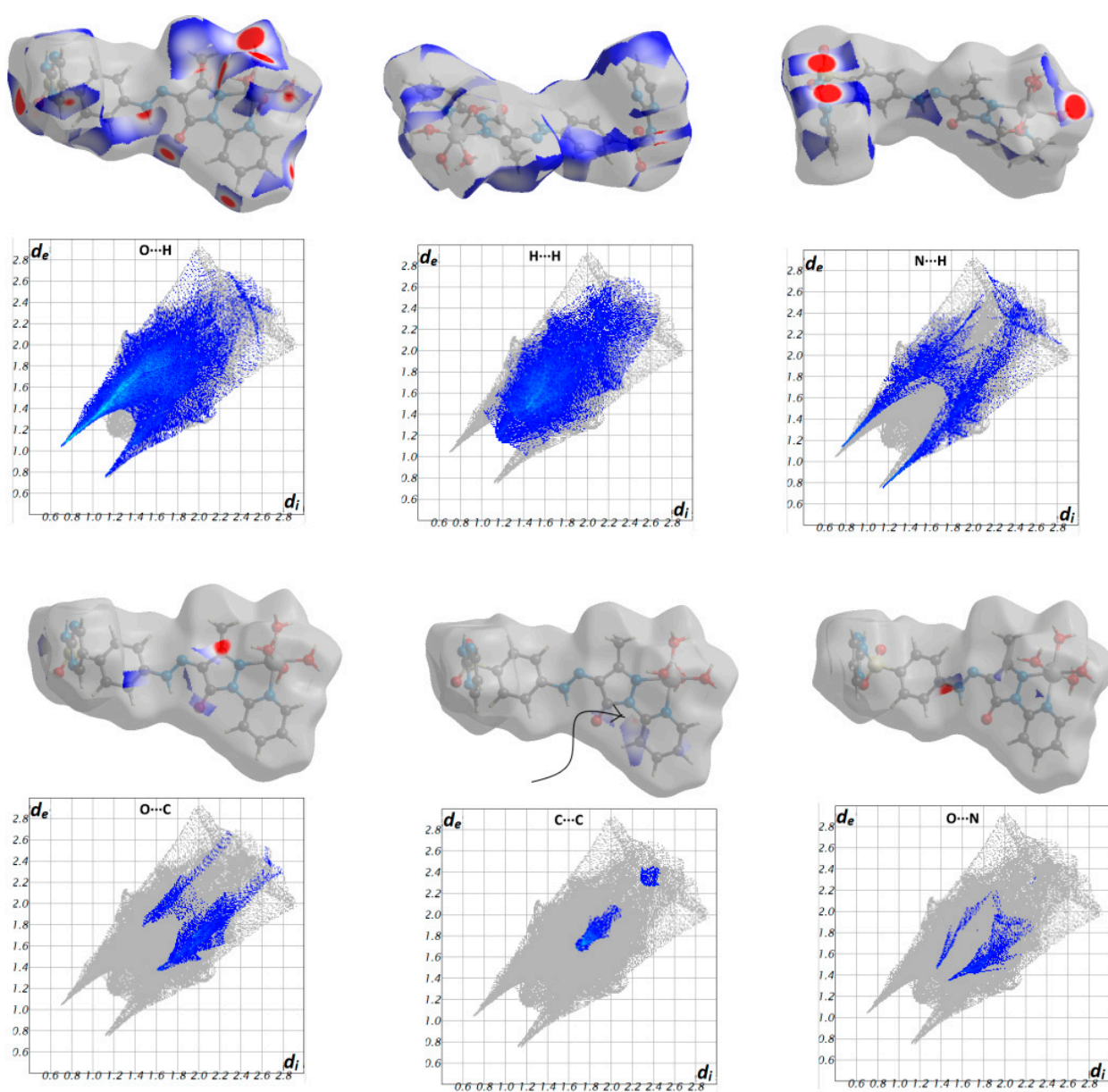


**Figure 6.** The  $d_{\text{norm}}$  maps and fingerprint plots of the most significant contacts in the cationic complex unit  $[\text{Co}(\text{L})(\text{H}_2\text{O})_4]^{2+}$  (**F1**).



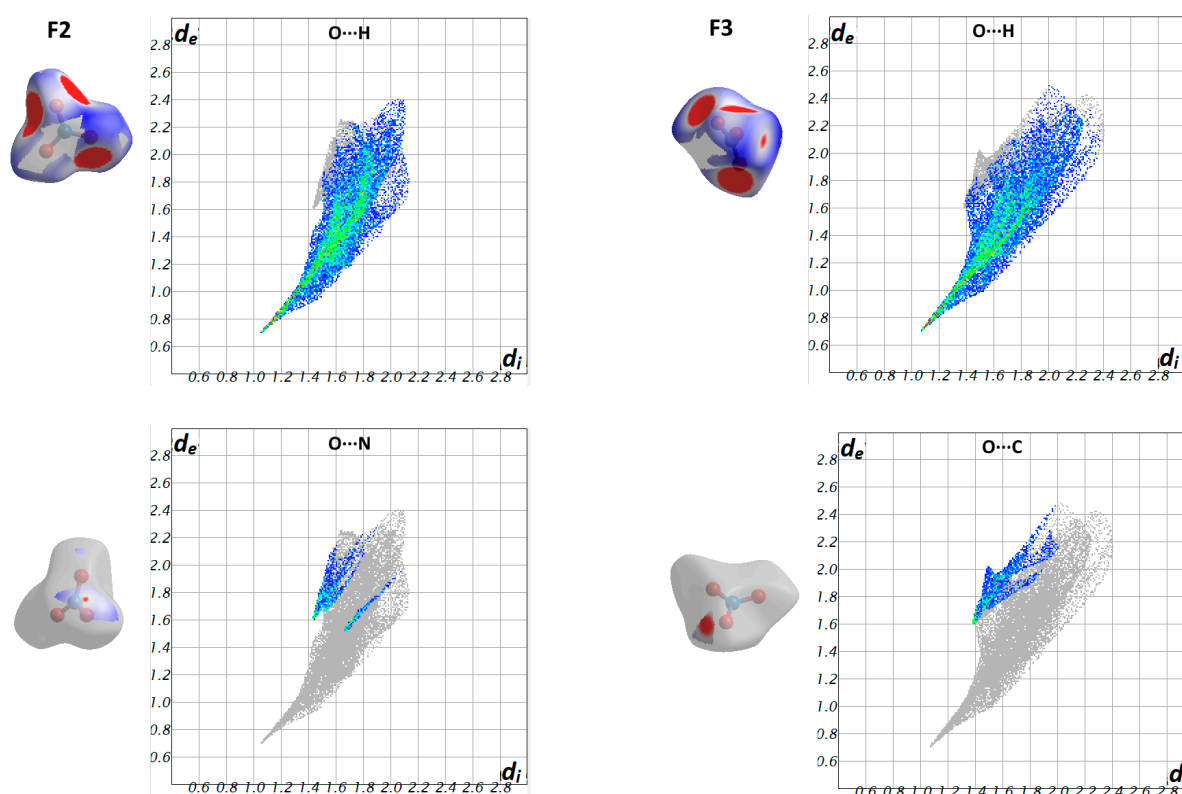


**Figure 7.** The  $d_{\text{norm}}$  maps and fingerprint plots for the most important interactions in the two nitrate anions (F2 and F3).

Additionally, the enrichment ratio which expressed the propensity of the atom pairs ( $X\cdots X$  or  $X\cdots Y$ ) to make contacts in the crystal was calculated based on the equations suggested by Jelsch and co-workers [36]. The percentage contribution of a given contact between two atom pairs, X and Y, is referred to as  $C_{XY}$ . Hence, the percentage contribution ( $S_X$ ) of an atom X on the Hirshfeld surface could be calculated using Equation (1).

$$S_X = C_{XX} + \frac{1}{2} \sum_{Y \neq X} C_{XY} \quad (1)$$

In the above equation, the  $C_{XY}$  includes the contact  $X\cdots Y$  and its reciprocal contact  $Y\cdots X$ . Hence, the sum of the  $S_X$  values is equal to unity ( $\sum_X S_X = 1$ ). The ratio of random contacts,  $R_{XX}$  and  $R_{XY}$ , between the elements X and Y could be calculated based on the relations  $R_{XX} = S_X S_X$  and  $R_{XY} = 2S_X S_Y$ , respectively. Furthermore, the sum of the ratios of the random contacts should be unity ( $\sum_X R_{XX} + \sum_{X \neq Y} R_{XY} = 1$ ). Then, the enrichment ratio could be calculated based on the ratio between the percentage contributions  $C_{XX}$  or  $C_{XY}$  to the ratio of random contacts  $R_{XX}$  and  $R_{XY}$ , respectively. The magnitude of the enrichment ratio ( $E_{XY}$ ) is generally more than 1 when two atom pairs have a high propensity for forming contacts in crystals. In contrast, the enrichment ratio ( $E_{XY}$ ) being less than 1 indicates atom pairs which tend to avoid contacts with each other in a crystal. The results of the enrichment ratio calculations for the fragment  $[\text{Co}(\text{L})(\text{H}_2\text{O})_4]^{2+}$  (F1) are depicted in Table 4. The enrichment ratio is greater than 1 for the  $\text{O}\cdots\text{H}$ ,  $\text{N}\cdots\text{C}$ ,  $\text{N}\cdots\text{H}$ , and  $\text{C}\cdots\text{C}$  contacts, revealing the high propensity of each atom pair for making interactions in the studied crystal structure. In contrast, the  $\text{O}\cdots\text{O}$ ,  $\text{O}\cdots\text{N}$ ,  $\text{O}\cdots\text{C}$ ,  $\text{C}\cdots\text{H}$ , and  $\text{H}\cdots\text{H}$  contacts have enrichment ratios less than 1, revealing the low propensity of each atom pair for forming contacts in the crystal structure.

**Table 4.** Results of the enrichment ratio  $\epsilon$  calculations for  $[\text{Co}(\text{L})(\text{H}_2\text{O})_4]^{2+}$  (**F1**).

| X...X/X...Y | C    | R     | E    | Atom | S     |
|-------------|------|-------|------|------|-------|
| O...O       | 0.9  | 5.74  | 0.16 | O    | 23.95 |
| O...N       | 2.1  | 3.71  | 0.57 | H    | 57.15 |
| O...C       | 5.2  | 5.34  | 0.97 | N    | 7.75  |
| O...H       | 38.8 | 27.37 | 1.42 | C    | 11.15 |
| N...N       | 0.6  | -     | -    |      |       |
| N...C       | 2.3  | 1.73  | 1.33 |      |       |
| N...H       | 9.9  | 8.86  | 1.12 |      |       |
| C...C       | 2.4  | 1.24  | 1.93 |      |       |
| C...H       | 10   | 12.74 | 0.78 |      |       |
| H...H       | 27.8 | 32.66 | 0.85 |      |       |

#### 2.4. Antimicrobial Studies

Testing the free ligand and its Co(II) complex against Gram-positive bacteria; *Staphylococcus aureus* (*S. aureus*) and Methicillin-resistant *Staphylococcus aureus* (MRSA (1)), and Gram-negative bacteria; *Klebsiella pneumonia* (*K. pneumonia*), *Proteus mirabilis* (*P. mirabilis*), *Acinetobacter baumannii* (*A. baumannii* (8)), and *Escherichia coli* (*E. coli*) was performed using DMSO as solvent, and the results were compared with Amoxicillin used as a positive antibacterial control. The antibacterial efficacy was determined by evaluating the minimum inhibitory concentrations (MIC) for these bacteria. The results of the MICs are listed in Table 5. The MIC data revealed that the free ligand had more antibacterial efficacy towards all the investigated bacteria and had lower MIC values (MIC = 62.5–125  $\mu\text{g/mL}$ ) than its Co(II) complex (MIC  $\geq$  250  $\mu\text{g/mL}$ ). In comparison to Amoxicillin, the MIC values confirmed the potency of the free ligand (MIC = 62.5–125  $\mu\text{g/mL}$ ) against all the tested bacteria, except *S. aureus* with an MIC value of  $\leq 7.8$   $\mu\text{g/mL}$ . In contrast, the Co(II) complex showed only promising results against *E. coli* (MIC = 250  $\mu\text{g/mL}$ ) compared to Amoxicillin (MIC > 500  $\mu\text{g/mL}$ ).

**Table 5.** MICs ( $\mu\text{g/mL}$ ) of the  $[\text{Co}(\text{L})(\text{H}_2\text{O})_4](\text{NO}_3)_2$  complex and its free ligand.

| Tested Compound                   | L    | $[\text{Co}(\text{L})(\text{H}_2\text{O})_4](\text{NO}_3)_2$ | Amoxicillin |
|-----------------------------------|------|--|-------------|
| <b>Gram-positive bacteria</b>     |      |  |             |
| <i>S. aureus</i> (ATCC 25923)     | 125  | >500   | $\leq 7.8$  |
| MRSA (1)                          | 125  | 500  | >500        |
| <b>Gram-negative bacteria</b>     |      |  |             |
| <i>E. coli</i> (ATCC 25922)       | 125  | 250  | >500        |
| <i>K. pneumonia</i> (ATCC 700603) | 125  | >500   | >500        |
| <i>P. mirabilis</i>               | 125  | >500   | 125         |
| <i>A. baumannii</i> (8)           | 62.5 | 500  | >500        |

### 3. Materials and Methods

#### 3.1. Chemicals and Instrumentations

All the chemicals and solvents were purchased from Sigma-Aldrich Company. Using a model 2400 instrument (Inc.940 Winter Street, Waltham, MA, USA), elemental analyses (CHN) were performed. Tensor 37 FTIR equipment (Waltham, MA, USA) was used to measure the FTIR spectra at 4000–400  $\text{cm}^{-1}$  in KBr pellets. Using a Shimadzu atomic absorption spectrophotometer (AA-7000 series, Shimadzu, Ltd., Tokyo, Japan), the amount of Co was measured.

#### 3.2. Syntheses

According to the described method mentioned by our research team [15], the ligand was prepared.

### Synthesis of $[\text{Co}(\text{L})(\text{H}_2\text{O})_4](\text{NO}_3)_2$ Complex

A 10 mL ethanolic solution of the ligand (43.6 mg, 0.1 mmol) was added to 29.1 mg of  $\text{Co}(\text{NO}_3)_2 \cdot 6\text{H}_2\text{O}$  (0.1 mmol) in 10 mL of ethanol. The resulting mixture was heated under reflux for 2 hr. The resulting clear, dark pink colored solution was filtered and allowed to evaporate at room temperature. Suitable dark pink crystals were collected after 4 weeks and were analyzed using a single-crystal X-ray diffraction analysis.

Yield: 85%; Anal. Calc.  $\text{C}_{19}\text{H}_{24}\text{CoN}_{10}\text{O}_{13}\text{S}$ : C, 33.00; H, 3.50; N, 20.26; Co, 8.52%. Found: C, 33.27; H, 3.35; N, 20.48; Co, 8.69%.  $[\text{Co}(\text{L})(\text{H}_2\text{O})_4](\text{NO}_3)_2$ . FTIR  $\text{cm}^{-1}$ : 3391, 1675, 1624, 1551, 1483, 1383, 1158, 936, 780, and 577. Ligand (L) FTIR  $\text{cm}^{-1}$ : 3430, 3071, 3020, 2927, 2864, 1679, 1598, 1553, 1473, 1434, 1337, 1257, 1156, 932, 734, 702, and 570 (Figure S1).

### 3.3. Crystal Structure Determination

The method indicated in the Supplementary Materials (Method S1) [37–41] was used to determine the crystal structure of the  $[\text{Co}(\text{L})(\text{H}_2\text{O})_4](\text{NO}_3)_2$  complex. Table 6 provides a summary of the crystal data and structure refinements.

**Table 6.** Crystal data of  $[\text{Co}(\text{L})(\text{H}_2\text{O})_4](\text{NO}_3)_2$  complex.

| CCDC                                       | 2282609  |
|--|--|
| empirical formula                          | $\text{C}_{19}\text{H}_{24}\text{CoN}_{10}\text{O}_{13}\text{S}$ |
| fw   | 691.47   |
| temp (K)                                   | 170(2)   |
| $\lambda$ (Å)                              | 0.71073  |
| cryst syst                                 | Triclinic  |
| space group                                | $P\bar{1}$   |
| $a$ (Å)                                    | 7.73330(10)  |
| $b$ (Å)                                    | 12.5152(2)   |
| $c$ (Å)                                    | 15.5216(2)   |
| $\alpha$ (deg)                             | 76.2120(10)  |
| $\beta$ (deg)                              | 77.9620(10)  |
| $\gamma$ (deg)                             | 78.9690(10)  |
| $V$ (Å <sup>3</sup> )                      | 1410.92(4)   |
| $Z$  | 2  |
| $\rho_{\text{calc}}$ (Mg/m <sup>3</sup> )  | 1.628  |
| $\mu$ (Mo K $\alpha$ ) (mm <sup>−1</sup> ) | 0.765  |
| No. reflns.                                | 50692  |
| Unique reflns.                             | 14152  |
| Completeness to $\theta = 25.242^\circ$    | 99.8%  |
| GOOF ( $F^2$ )                             | 1.028  |
| $R_{\text{int}}$                           | 0.0239   |
| $R_1^a$ ( $I \geq 2\sigma$ )               | 0.0416   |
| $wR_2^b$ ( $I \geq 2\sigma$ )              | 0.1172   |

$$^a R_1 = \sum ||F_o| - |F_c|| / \sum |F_o|, \quad ^b wR_2 = \{\sum [w(F_o^2 - F_c^2)^2] / \sum [w(F_o^2)^2]\}^{1/2}.$$

### 3.4. Hirshfeld Surface Analysis

To create 2D fingerprint plots and Hirshfeld surfaces [42] for the topological analysis, the Crystal Explorer 17.5 software [43] was used.

### 3.5. Antimicrobial Studies

According to Method S2 (Supplementary Materials) [44], the antibacterial activities of the studied ligand and its Co(II) complex were assessed.

## 4. Conclusions

In this research, a new self-assembled  $[\text{Co}(\text{L})(\text{H}_2\text{O})_4](\text{NO}_3)_2$  complex of a sulfadiazine-pyrazole derivative (L) was synthesized and analyzed using several experimental (FTIR, elemental analysis, and single-crystal X-ray diffraction) and theoretical (Hirshfeld analysis)

techniques. The crystal structure of this complex was confirmed using a single-crystal X-ray diffraction analysis. The Co(II) ion was coordinated with four O-atoms from the four water molecules and two N-atoms from the bidentate ligand in a distorted octahedral coordination environment. The intermolecular interactions of the different fragments of this complex were analyzed with the aid of a Hirshfeld surface analysis. The O...H (38.8%), H...H (27.8%), and N...H (9.9%) hydrogen bonds represented the majority of interactions for the cationic inner sphere  $[\text{Co}(\text{L})(\text{H}_2\text{O})_4]^{2+}$ . The predominant contacts for the counter  $\text{NO}_3^-$  anions were the O...H, O...N, and O...C contacts. The atom pairs in the O...H, N...C, N...H, and C...C contacts had a high propensity for making interactions, as revealed by their greater enrichment ratio than 1. The complex and free ligand's antibacterial effectiveness were examined. The free ligand exhibited greater antibacterial activity ( $\text{MIC} = 62.5 \geq 125 \mu\text{g/mL}$ ) than the  $[\text{Co}(\text{L})(\text{H}_2\text{O})_4](\text{NO}_3)_2$  complex ( $\text{MIC} \geq 250 \mu\text{g/mL}$ ) against all the bacteria under study.

**Supplementary Materials:** The following supporting information can be downloaded at: <https://www.mdpi.com/article/10.3390/inorganics11100382/s1>, Figure S1: FTIR spectra of the ligand L (upper) and  $[\text{Co}(\text{L})(\text{H}_2\text{O})_4](\text{NO}_3)_2$  complex (lower); Method S1: Crystal Structure Determination; Method S2: Antibacterial activity assay.

**Author Contributions:** Conceptualization, S.M.S., M.S.A. (Mohammed Salah Ayoup) and M.A.M.A.-Y.; methodology, A.Y. and M.S.A. (Mohammed Salah Ayoup); software, M.H., S.M.S. and M.S.A. (Mezna Saleh Altowyan); validation, A.Y., A.B., S.M.S. and M.H.; formal analysis, A.Y., M.M.F.I., N.G.E.M., M.M.S. and M.S.A. (Mezna Saleh Altowyan); investigation, A.Y., M.S.A. (Mohammed Salah Ayoup) and S.M.S.; resources, M.S.A. (Mohammed Salah Ayoup) and A.B.; data curation, M.H. and S.M.S.; writing—original draft preparation, S.M.S., A.B. and A.Y.; writing—review and editing, A.Y., A.B., S.M.S., M.S.A. (Mezna Saleh Altowyan) and M.H.; visualization, A.Y., M.S.A. (Mohammed Salah Ayoup), M.A.M.A.-Y. and A.B.; supervision, S.M.S. and M.A.M.A.-Y.; funding acquisition, M.S.A. (Mezna Saleh Altowyan). All authors have read and agreed to the published version of the manuscript.

**Funding:** Princess Nourah bint Abdulrahman University Researchers Supporting Project number (PNURSP2023R86), Princess Nourah bint Abdulrahman University, Riyadh, Saudi Arabia.

**Data Availability Statement:** Not Applicable.

**Acknowledgments:** Princess Nourah bint Abdulrahman University Researchers Supporting Project number (PNURSP2023R86), Princess Nourah bint Abdulrahman University, Riyadh, Saudi Arabia.

**Conflicts of Interest:** The authors declare no conflict of interest.

## References

- Koshti, S.M.; Patil, P.A.; Patil, C.B.; Patil, A.S. Synthesis and characterization of prodrugs of sulfonamides as an azo derivatives of carvacrol. *Pharma. Chem.* **2018**, *10*, 1–15.
- Pradere, U.; Garnier-Amblard, E.C.; Coats, S.J.; Amblard, F.; Schinazi, R.F. Synthesis of nucleoside phosphate and phosphonate prodrugs. *Chem. Rev.* **2014**, *114*, 9154–9218. [\[CrossRef\]](#)
- Connor, E.E. Sulfonamide antibiotics. *Prim. Care Update Ob/Gyns* **1998**, *5*, 32–35. [\[CrossRef\]](#)
- Venkatesan, M.; Fruci, M.; Verellen, L.A.; Skarina, T.; Mesa, N.; Flick, R.; Pham, C.; Mahadevan, R.; Stogios, P.J.; Savchenko, A. Molecular mechanism of plasmid-borne resistance to sulfonamide antibiotics. *Nat. Commun.* **2023**, *14*, 4031. [\[CrossRef\]](#) [\[PubMed\]](#)
- Gil, D.M.; Pérez, H.; Echeverría, G.A.; Piro, O.E.; Frontera, A. Role of imidazole co-ligand in the supramolecular network of a Co(II) complex with sulfadiazine: Crystal structure, Hirshfeld surface analysis and energetic calculations. *ChemistrySelect* **2020**, *5*, 6331–6338. [\[CrossRef\]](#)
- Yang, X.-L.; Liu, J.; Yang, L.; Zhang, X.-Y. Synthesis, characterization, and susceptibility of bacteria of selenium dioxide complexes with sulfadiazine. *Synth. React. Inorg. Met.* **2005**, *35*, 761–766. [\[CrossRef\]](#)
- El-Baradie, K.; Gaber, M. Synthesis, spectral, thermal, and electrical conductivity studies of cobalt(II) and copper(II) sulfadiazine complexes. *Chem. Pap.* **2003**, *57*, 317–321.
- Shi, W.-B.; Cui, A.-L.; Kou, H.-Z. Sulfadiazine/dimethylsulfadiazine transition metal complexes: Synthesis, crystal structures and magnetic properties. *Polyhedron* **2015**, *99*, 252–259. [\[CrossRef\]](#)
- Schapira, A.; Beales, P.; Halloran, M. Malaria: Living with drug resistance. *Parasitol. Today* **1993**, *9*, 168–174. [\[CrossRef\]](#)
- Fernández-Villa, D.; Aguilar, M.R.; Rojo, L. Folic acid antagonists: Antimicrobial and immunomodulating mechanisms and applications. *Int. J. Mol. Sci.* **2019**, *20*, 4996. [\[CrossRef\]](#)

11. Mani, F. Model systems containing pyrazole chelates and related groups: Recent developments and perspectives. *Coord. Chem. Rev.* **1992**, *120*, 325–359. [\[CrossRef\]](#)
12. Trofimenko, S. Coordination chemistry of pyrazole-derived ligands. *Chem. Rev.* **1972**, *72*, 497–509. [\[CrossRef\]](#)
13. Seth, S.K.; Saha, N.C.; Ghosh, S.; Kar, T. Structural elucidation and electronic properties of two pyrazole derivatives: A combined X-ray, Hirshfeld surface analyses and quantum mechanical study. *Chem. Phys. Lett.* **2011**, *506*, 309–314. [\[CrossRef\]](#)
14. Shafiq, N.; Shahzad, N.; Rida, F.; Ahmad, Z.; Nazir, H.A.; Arshad, U.; Zareen, G.; Attiq, N.; Parveen, S.; Rashid, M. One-pot multicomponent synthesis of novel pyridine derivatives for antidiabetic and antiproliferative activities. *Future Med. Chem.* **2023**, *15*. [\[CrossRef\]](#)
15. Altowyan, M.S.; Soliman, S.M.; Ismail, M.M.; Haukka, M.; Barakat, A.; Ayoup, M.S. New bioprecursor prodrugs of sulfadiazine: Synthesis, X-ray structure and Hirshfeld analysis. *Crystals* **2022**, *12*, 1016. [\[CrossRef\]](#)
16. Wong, E.; Giandomenico, C.M. Current status of platinum-based antitumor drugs. *Chem. Rev.* **1999**, *99*, 2451–2466. [\[CrossRef\]](#)
17. Ott, I.; Gust, R. Non platinum metal complexes as anti-cancer drugs. *Arch. Pharm. Int. J. Pharm. Med. Chem.* **2007**, *340*, 117–126. [\[CrossRef\]](#)
18. Northcote-Smith, J.; Suntharalingam, K. Targeting chemotherapy-resistant tumour sub-populations using inorganic chemistry: Anti-cancer stem cell metal complexes. *Curr. Opin. Chem. Biol.* **2023**, *72*, 102237. [\[CrossRef\]](#)
19. Nasiri Sovari, S.; Zobi, F. Recent studies on the antimicrobial activity of transition metal complexes of groups 6–12. *Chemistry* **2020**, *2*, 418–452. [\[CrossRef\]](#)
20. Fahim, A.M.; Hasanin, M.; Habib, I.; El-Attar, R.O.; Dacrory, S. Synthesis, antimicrobial activity, theoretical investigation, and electrochemical studies of cellulosic metal complexes. *J. Iran. Chem. Soc.* **2023**, *20*, 1699–1718. [\[CrossRef\]](#)
21. Yousri, A.; El-Faham, A.; Haukka, M.; Ayoup, M.S.; Ismail, M.M.; Menofy, N.G.E.; Soliman, S.M.; Öhrström, L.; Barakat, A.; Abu-Youssef, M.A. A novel Na(I) coordination complex with *s*-triazine pincer ligand: Synthesis, X-ray structure, Hirshfeld analysis, and antimicrobial activity. *Crystals* **2023**, *13*, 890. [\[CrossRef\]](#)
22. Yousry, A.; Haukka, M.; Abu-Youssef, M.A.; Ayoup, M.S.; Ismail, M.M.; El Menofy, N.; Soliman, S.M.; Barakat, A.; Noa, F.M.A.; Öhrström, L.R. Synthesis, structure diversity, and antimicrobial studies of Ag(I) complexes with quinoline-type ligands. *CrystEngComm* **2023**, *25*, 3922–3930. [\[CrossRef\]](#)
23. García-Raso, Á.; Fiol, J.J.; Rigo, S.; López-López, A.; Molins, E.; Espinosa, E.; Borrás, E.; Alzuet, G.; Borrás, J.N.; Castiñeiras, A. Coordination behaviour of sulfanilamide derivatives.: Crystal structures of [Hg(sulfamethoxypyridazinato)<sub>2</sub>], [Cd(sulfadimidinato)<sub>2</sub>(H<sub>2</sub>O)].2H<sub>2</sub>O and [Zn (sulfamethoxazolato)<sub>2</sub>-(pyridine)<sub>2</sub>(H<sub>2</sub>O)<sub>2</sub>]. *Polyhedron* **2000**, *19*, 991–1004. [\[CrossRef\]](#)
24. Hossain, G.G.; Amoroso, A.; Banu, A.; Malik, K. Syntheses and characterisation of mercury complexes of sulfadiazine, sulfamerazine and sulfamethazine. *Polyhedron* **2007**, *26*, 967–974. [\[CrossRef\]](#)
25. Villa-Pérez, C.; Oyarzabal, I.; Echeverría, G.A.; Valencia-Urbe, G.C.; Seco, J.M.; Soria, D.B. Single-ion magnets based on mononuclear cobalt(II) complexes with sulfadiazine. *Eur. J. Inorg. Chem.* **2016**, *2016*, 4835–4841. [\[CrossRef\]](#)
26. Brown, C.; Cook, D.; Sengier, L. Bis[N<sup>1</sup>-(2-pyrimidinyl)sulphanilamido]zinc-ammonia (1/2), [Zn(C<sub>10</sub>H<sub>9</sub>N<sub>4</sub>O<sub>2</sub>S)<sub>2</sub>].2NH<sub>3</sub>. *Acta Crystallogr. C Cryst. Struct. Commun.* **1985**, *41*, 718–720. [\[CrossRef\]](#)
27. Greenhalgh, D.G. Topical antimicrobial agents for burn wounds. *Clin. Plast. Surg.* **2009**, *36*, 597–606. [\[CrossRef\]](#)
28. Fox, C.L. Silver sulfadiazine—a new topical therapy for pseudomonas in burns: Therapy of pseudomonas infection in burns. *Arch. Surg.* **1968**, *96*, 184–188. [\[CrossRef\]](#)
29. Fox, C.L.; Modak, S.; Stanford, J.; Fox, P.L. Metal sulfonamides as antibacterial agents in topical therapy. *Scand. J. Plast. Reconstr. Surg.* **1979**, *13*, 89–94. [\[CrossRef\]](#)
30. Ajibade, P.A.; Kolawole, G.A.; O'Brien, P.; Helliwell, M.; Raftery, J. Cobalt(II) complexes of the antibiotic sulfadiazine, the X-ray single crystal structure of [Co(C<sub>10</sub>H<sub>9</sub>N<sub>4</sub>O<sub>2</sub>S)<sub>2</sub>(CH<sub>3</sub>OH)<sub>2</sub>]. *Inorg. Chim. Acta* **2006**, *359*, 3111–3116. [\[CrossRef\]](#)
31. Rocha, M.; Piro, O.E.; Echeverría, G.A.; Pastoriza, A.C.; Sgariglia, M.A.; Soberón, J.R.; Gil, D.M. Co(II), Ni(II) and Cu(II) ternary complexes with sulfadiazine and dimethylformamide: Synthesis, spectroscopic characterization, crystallographic study and antibacterial activity. *J. Mol. Struct.* **2019**, *1176*, 605–613. [\[CrossRef\]](#)
32. Anaconda, J.; Noriega, N.; Camus, J. Synthesis, characterization and antibacterial activity of a tridentate schiff base derived from cephalothin and sulfadiazine, and its transition metal complexes. *Spectrochim. Acta A Mol. Biomol. Spectrosc.* **2015**, *137*, 16–22. [\[CrossRef\]](#) [\[PubMed\]](#)
33. Lutsenko, I.A.; Yambulatov, D.S.; Kiskin, M.A.; Nelyubina, Y.V.; Primakov, P.V.; Bekker, O.B.; Levitskiy, O.A.; Magdesieva, T.V.; Imshennik, V.K.; Maksimov, Y.V. Improved in vitro antimycobacterial activity of trinuclear complexes cobalt(II, III) and iron(III) with 2-furoic acid against mycolicibacterium smegmatis. *ChemistrySelect* **2020**, *5*, 11837–11842. [\[CrossRef\]](#)
34. Chadghan, A.; Pons, J.; Caubet, A.; Casabó, J.; Ros, J.; Alvarez-Larena, A.; Piniella, J.F. Cobalt(II) complexes with pyrazole-derived ligands: Crystal structure of [bis [3-phenyl-5-(2-pyridyl) pyrazole] aquachlorocobalt(II)] chloride monohydrate. *Polyhedron* **2000**, *19*, 855–862. [\[CrossRef\]](#)
35. Liu, C.-S.; Zhang, H.; Chen, R.; Shi, X.-S.; Bu, X.-H.; Yang, M. Two new Co(II) and Ni(II) complexes with 3-(2-pyridyl) pyrazole-based ligand: Synthesis, crystal structures, and bioactivities. *Chem. Pharm. Bull.* **2007**, *55*, 996–1001. [\[CrossRef\]](#)
36. Jelsch, C.; Ejsmont, K.; Hudera, L. The enrichment ratio of atomic contacts in crystals, an indicator derived from the Hirshfeld surface analysis. *IUCrJ* **2014**, *1*, 119–128. [\[CrossRef\]](#)
37. Rikagu Oxford Diffraction. *CrysAlisPro*; Rikagu Oxford Diffraction Inc.: Yarnton, UK, 2020.
38. Sheldrick, G. *Sadabs-Bruker Nonius Scaling and Absorption Correction*; Bruker AXS Inc.: Madison, WI, USA, 2012.



39. Sheldrick, G.M. Shelxt–integrated space-group and crystal-structure determination. *Acta Cryst.* **2015**, *A71*, 3–8. [[CrossRef](#)]
40. Sheldrick, G.M. Crystal structure refinement with SHELXL. *Acta Cryst.* **2015**, *C71*, 3–8.
41. Hübschle, C.B.; Sheldrick, G.M.; Dittrich, B. A Qt Graphical User Interface for SHELXL. *J. Appl. Cryst.* **2011**, *44*, 1281–1284. [[CrossRef](#)]
42. Hirshfeld, F.L. Bonded-atom fragments for describing molecular charge densities. *Theor. Chim. Acta* **1977**, *44*, 129–138. [[CrossRef](#)]
43. Mackenzie, C.F.; Spackman, P.R.; Jayatilaka, D.; Spackman, M.A. Crystalexplorer model energies and energy frameworks: Extension to metal coordination compounds, organic salts, solvates and open-shell systems. *IUCr* **2017**, *4*, 575–587. [[CrossRef](#)] [[PubMed](#)]
44. Wayne, P. Clinical and Laboratory Standards Institute: Performance Standards for Antimicrobial Susceptibility Testing: 20th Informational Supplement. CLSI Document M100-S20. *Kansenshogakuzasshi* **2010**, *85*, 355–359. [[CrossRef](#)]

**Disclaimer/Publisher’s Note:** The statements, opinions and data contained in all publications are solely those of the individual author(s) and contributor(s) and not of MDPI and/or the editor(s). MDPI and/or the editor(s) disclaim responsibility for any injury to people or property resulting from any ideas, methods, instructions or products referred to in the content.